2 Overview of radiation effects on detector systems

I. Dawson[a], *F. Faccio*[b], *M. Moll*[b], *A. Weidberg*[c]
[a]Queen Mary University of London, United Kingdom
[b]CERN, Geneva, Switzerland
[c]University of Oxford, United Kingdom

In this section we give an overview of the effects of radiation on silicon detector systems in the LHC experiments. We divide the sections into: sensors; electronics; optoelectronics; services. While the physics of the energy loss between these categories is similar, the radiation quantities of interest used to evaluate damage are usually different. As an example, sensor radiation studies typically focus on the effects of bulk displacement damage, whereas degradation in electronics is generally more concerned with ionizing dose effects.

2.1 Sensors

The various sensor types employed in the LHC experiments suffer from radiation induced performance degradation that is mostly originating from displacement damage effects occurring in the silicon bulk of the devices. In this section, we present a general overview of displacement damage effects with relevance for all silicon sensor types. The given data were mainly obtained on very simple sensor structures, so-called pad detectors with single electrodes on the top and bottom of a silicon layer, that allow for an in-depth investigation of the bulk damage effects. For more complex sensor geometries with surface passivation layers or AC-coupled readout, additional damage effects might have to be considered. These are described in the experiment specific sections. This section starts with an introduction to the non-ionizing energy loss theorem and a description of the properties of electrically active radiation induced defects in the framework of the Shockley–Read–Hall theory. Then, the main macroscopic damage effects observed as increase of leakage current, change of effective doping concentration, and loss of charge collection efficiency are presented. Finally, a brief introduction to the radiation induced change of the sensor internal electrical field shape is given, pointing towards the full complexity of the understanding of radiation damage effects in segmented silicon sensors.

2.1.1 Non-ionizing energy loss

The non-ionizing energy loss (NIEL) gives the portion of energy lost by a traversing particle which does not go into ionization and eventually leads to displacement damage. However, only a fraction of the NIEL leads to displacements as part of the energy is dissipated in phonons. This fraction depends on the energy of the impinging particle. NIEL is defined in units of MeVcm^2/g or as NIEL cross-section (displacement damage function D) in units of MeVmb. A reference value of 1 MeV neutron equivalent (n_{eq}) has been fixed to 95 MeVmb. Calculated values of the NIEL cross-sections for various particles are shown in Fig. 1. The NIEL hypothesis assumes that radiation damage effects scale linearly with NIEL, irrespective of the distribution of the primary displacements over energy and space. For the simulated examples shown in Fig. 2 the number of vacancies should give a measure of the damage irrespective of their distribution, whether homogeneously scattered over a relatively wide volume (as for the case of low energetic proton or gamma-ray damage) or clustered in high density in small regions (as in the case of neutron damage). Consequently, the damage produced by different particles or particles with

This chapter should be cited as: Overview of radiation effects on detector systems, Eds. I. Dawson, M. Moll, F. Faccio, A. Weidberg, DOI: 10.23731/CYRM-2021-001.3, in: Radiation effects in the LHC experiments: Impact on detector performance and operation, Ed. Ian Dawson,
CERN Yellow Reports: Monographs, CERN-2021-001, DOI: 10.23731/CYRM-2021-001, p. 3.

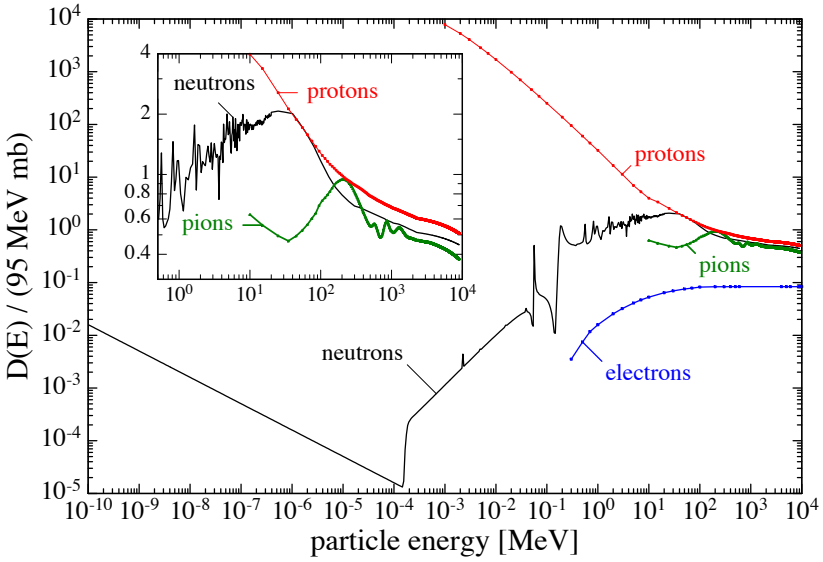

Fig. 1: Non-ionizing energy loss (NIEL) cross-sections normalized to 95 MeV mb. Data collected by A.Vasilescu and G.Lindström [1] based on [2–5] and private communications.

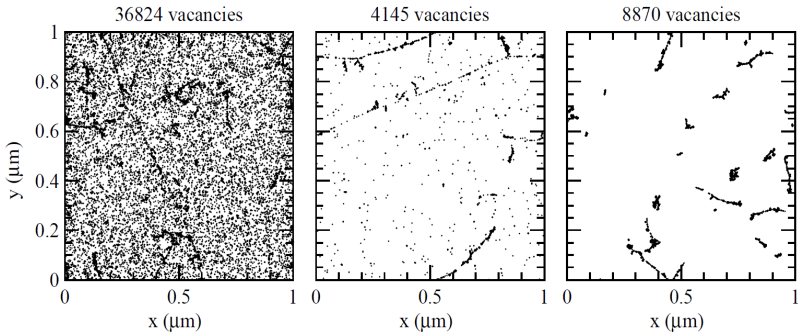

Fig. 2: Initial distribution of vacancies produced by 10 MeV protons (left), 23 GeV protons (middle), and 1 MeV neutrons (right). The plots are projected over 1 μm depth (z) and correspond to a fluence of 10^{14} particles/cm^2. Figure taken from Ref. [6].

different energies should be scalable via their NIEL (i.e., the number of displacements) and the data given in Fig. 1 should allow us to normalize the damage from different particles or particles with different energies. As will be shown below, NIEL scaling is a powerful method for coping with displacement damage predictions in complex radiation fields. It allows us to predict many device damage parameters in fast hadron dominated radiation fields (such as, e.g., the leakage current) but also has shortcomings arising, for example, from the fact that point-like and clustered defects contribute differently to some device damage parameters such as, e.g., the effective space charge (see Section 2.1.2). The displacement damage functions shown in Fig. 1 are presently used to calculate the 1 MeV neutron equivalent fluence radiation fields in the experiments of the LHC and HL-LHC. It has, however, been shown that, for protons and electrons, an *effective NIEL* [7, 8] or the *equivalent displacement damage dose* concept [8–10] can deliver better linearity between some damage parameters and the calculated NIEL (see e.g., Ref. [11]). A revision of the used damage functions for the 1 MeV neutron equivalent fluence calculation is thus of interest.

2.1.2 Radiation induced defects

Radiation induced electrically active defects with energy levels in the silicon bandgap impact on the device performance in various ways. Generally, the impact on the detector performance can be described in the framework of the Shockley–Read–Hall (SRH) statistics and, in principle, the impact of each defect can be calculated if the capture cross-sections for holes σ_p and electrons σ_n, the position in the bandgap, the type of defect (acceptor or donor), and the concentration of the defect N_t are known (see, e.g., Ref. [12]). On the device performance level, three main effects can be identified and are discussed in the following with their formulation in the SRH framework.

Leakage current: The leakage current is most effectively produced by defect levels close to the middle of the bandgap. It follows the NIEL hypothesis scaling for high energy hadron induced damage, meaning as well that defect engineering (i.e., the impurity content of the silicon) has in this case no impact on the leakage current (see e.g., Ref. [14]). Increase of leakage current leads to an increase of noise in the amplifiers and to an increase of power consumption. As the leakage current depends exponentially on the temperature, cooling is a very effective means to mitigate the detrimental effects. To calculate the leakage current, we need to determine the defect occupancy with electrons f_t given by

$$f_t = \frac{c_n n + e_p}{c_n n + e_n + c_p p + e_p}\,, \tag{1}$$

where c_n and c_p are the capture coefficients for electrons and holes, n and p are the electron and hole densities, and e_n and e_p the emission rates for electrons and holes. The value of c_n is given by $c_n = \sigma_n v_{th,n}$, with $v_{th,n}$ being the thermal velocity for electrons and e_n being given by $e_n = c_n n_i \exp((E_t - E_i)/k_B T)$, with n_i being the intrinsic carrier density, E_i the intrinsic Fermi level, and k_B the Boltzmann constant. In the space charge region (SCR) of a detector the carrier densities are very low and can often be neglected, simplifying Eq. 1 to

$$f_t = e_p/(e_n + e_p)\,. \tag{2}$$

Defect levels produce leakage current by the subsequent emission of electrons and holes (i.e., the transfer of electrons from the valence to the conduction band). The generation rate G_t of a single defect type t in the case of neglectable free carrier concentrations is given by

$$G_t = N_t f_t e_n = N_t(1 - f_t)e_p = N_t \frac{e_n e_p}{e_n + e_p}\,. \tag{3}$$

Summing over all defect types and taking into account the active volume of a sensor (depletion width w and area A) results in the total leakage of the device

$$I = q_0 w A \sum_{\text{defects}} G_t\,, \tag{4}$$

with q_0 being the elementary charge.

Effective space charge: In undamaged sensors, the bulk doping (e.g., phosphorus or boron) constitutes the effective space charge. Radiation induced changes to the effective space charge lead to a change of the electric field distribution within the device and shift the depletion voltage to lower or higher values. In the latter case, higher operation voltages might have to be applied to establish an electric field throughout the full sensor volume in order to avoid under-depletion and loss of active volume and therefore signal. If sufficiently high voltage cannot be applied or breakdown of the sensor is at risk, sensors will have to be operated under-depleted with the corresponding loss in signal heights. Inhomogeneous distribution of the space charge might lead to double junction effects or the shift of the highest electric field towards regions that are unprofitable for segmented sensors. High local fields can lead furthermore to impact ionization effects or breakdown. It has been shown that the change of the space charge in silicon is strongly material dependent (e.g., oxygen content) and depends on the particle type used for the irradiation experiment (e.g., neutron vs. proton damage). This implies that this damage effect does not directly scale with NIEL

and can be altered or mitigated by defect engineering approaches (e.g., change of impurity content). Defects can contribute positive (donors) or negative (acceptors) charge to the space charge and thus alter the electric field distribution and the depletion voltage of a device. The effective space charge N_{eff} (neglecting free carriers) is then given by the sum of all positively charged donors N_D and all negatively charged acceptors N_A

$$N_{\text{eff}} = \sum_{\text{donors}} (1 - f_t) N_t - \sum_{\text{acceptors}} f_t N_t \,, \tag{5}$$

where the index t is running over all donor and acceptor like defect type t with concentration N_t.

Trapping: Charge carriers generated by ionizing particles or photons in the SCR travel towards the electrodes and constitute the sensor signal. Defect levels can capture (trap) charge carriers and, if the release (detrapping) time of the charge carriers is long compared to the collection time of the system or if the concentration of defects (trapping centres) is very high, the overall signal of the sensor is reduced. Trapping becomes the limiting factor for high fluence applications. Mitigation of this problem is possible through device modifications leading to faster collection times (i.e., device engineering). In segmented sensors, the collection of electrons instead of holes at the sensing electrodes can be an advantage due to the higher mobility of electrons and the possibility of exploiting charge multiplication by impact ionization at lower fields and without device breakdown. The trapping is characterized by a trapping time (inverse capture rate) τ_e for electrons and τ_h for holes that are calculated as

$$1/\tau_e = c_n (1 - f_t) N_t \;\text{ and }\; 1/\tau_h = c_p f_t N_t \,. \tag{6}$$

Summing over all defects contributing to the trapping results in the effective trapping times τ_{eff} for electrons and holes

$$\frac{1}{\tau_{eff,e}} = \sum_{\text{defects}} c_{(n,t)} (1 - f_t) N_t \tag{7}$$

$$\frac{1}{\tau_{eff,h}} = \sum_{\text{defects}} c_{(p,t)} f_t N_t \,. \tag{8}$$

Equations 1 to 8 allow us to estimate the impact of defects (with known parameters of donor/acceptor, σ_n, σ_p, E_t and N_t) on the space charge, current generation, and trapping. For precise calculations, the defect parameters have to be properly embedded in the Poisson and transport equations, as done for example in technology computer aided design (TCAD) device simulations (see Chapter 7). This allows us to determine the device geometry, spatial distribution of defect concentrations, free carrier densities, field strength, and other semiconductor effects such as, for example, impact ionization.

2.1.3 Impact of radiation on sensor performance

Silicon particle detectors are basically reverse biased silicon diode structures. Correspondingly, the most simple test structure to investigate radiation damage effects on silicon detectors is the a so-called *pad detector*. It consists of a large front electrode (with respect to the thickness of the silicon bulk) surrounded by one or a series of guard rings (to protect the collecting electrodes from unwanted currents originating from the edges and to precisely define the active volume) and a homogeneous electrode covering all back side. For n-type bulk structures, the front contact and guard rings are p^+ implants and the backside implant is an n^+ implant. Typical dimensions are 5 mm $\times$ 5 mm for the front electrode and 300 μm for the thickness of the silicon bulk. Most of the results presented in the following sections are based on measurements on pad detectors. Segmented sensors add more complexity to the impact of bulk (and surface) radiation damage and will be treated at the end of the section and in the following chapters.

The principle radiation effects originating from displacement damage in the silicon bulk of the detectors are an increase in the leakage current (dark current), a change of the effective doping concentration (change of depletion voltage), and a decrease of the charge collection efficiency (i.e., a reduction

of the signal due to trapping effects). These effects are strongly interlinked and partly depend on the material parameters such as impurities in the silicon and/or do not follow the NIEL scaling concept. Therefore, the parameterization and damage parameters presented in the following section have to be carefully benchmarked against the experimental situation for which the modelling is applied. Especially after exposure to very high particle fluences, when the electric field inside the sensor is no longer a linear function of the distance from the collecting electrode, parameters like the depletion voltage can no longer serve to straightforwardly calculate the electric field and the charge collection efficiency.

2.1.3.1 Leakage current

Leakage current: Fluence dependence

After exposure to highly energetic particles having sufficient energy to produce so-called defect clusters (see e.g., Ref. [13]), the radiation induced increase of the leakage current is proportional to the particle fluence and independent of the type, resistivity, and impurity content of the used silicon material [14,15]. This is shown in Fig. 3 (left) for various silicon detectors [16]. The proportionality factor is called *current related damage factor* α and is defined by

$$\alpha = \frac{\Delta I}{V \phi_{\mathrm{eq}}}, \tag{9}$$

where ΔI is the leakage current increase caused by irradiation, V the volume contributing to the current, and ϕ_{eq} the 1 MeV neutron equivalent particle fluence. The data shown in Fig. 3 (left) result in a value of $\alpha(80\ \mathrm{min},\ 60\,^{\circ}\mathrm{C}) = (3.99 \pm 0.03) \times 10^{-17}$ A/cm for the measurements taken at 20 °C. It shall be

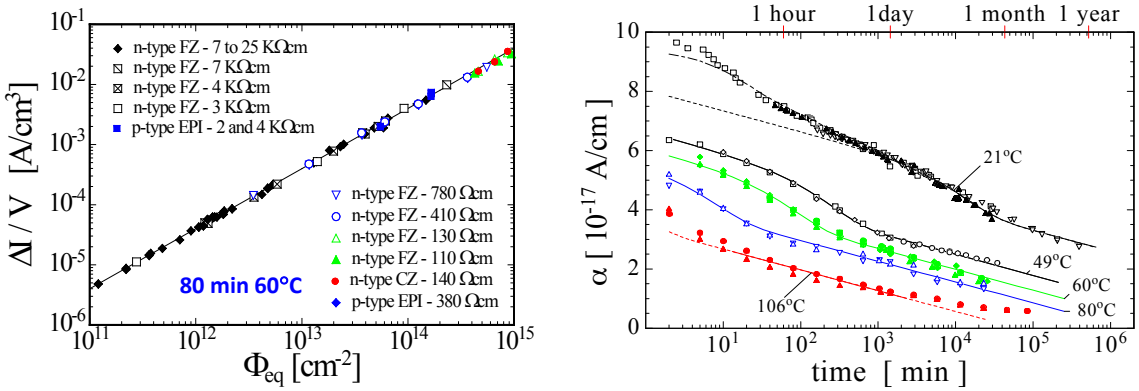

Fig. 3: Left: Radiation induced leakage current increase as a function of particle fluence for various silicon detectors made from silicon materials produced by various process technologies with different resistivities and conduction types. The current was measured at room temperature (20 °C) after irradiation in a neutron field with 5.2 MeV mean energy and a dedicated annealing of 80 min at 60 °C. Figure taken from Ref. [16]. Right: Current related damage rate α as a function of cumulated annealing time at different temperatures. Solid lines represent fits to the data (see text). Figure taken from Ref. [17].

mentioned that for irradiations producing predominantly point defects (e.g., ^{60}Co-gamma) a non-linear dependence on the particle fluence and a strong dependence on the impurity content are observed [18]. This case is not further treated here as in the LHC context the defect cluster induced leakage is the dominant one; more details regarding point-defect induced leakage can be found in Ref. [19].

Leakage current: Temperature dependence

The temperature dependence of the leakage current is dominated by the position of the energy levels in the band gap, their cross-sections, their concentrations, and the temperature dependence of the bandgap

itself. The most efficient generation centres are the ones at the intrinsic energy level. In this case, the leakage current temperature dependence will follow that of the intrinsic carrier concentration n_i. In a recent work, experimental results obtained on several different irradiated silicon particle detectors using the parameterization

$$I(T) \propto T^2 \exp\left(-E_{\text{eff}}/2k_BT\right) \tag{10}$$

were compared and resulted in a value of $E_{\text{eff}} = 1.214 \pm 0.014$ eV [20]. This value is presently the reference in the HEP community for temperature correction (scaling) of the leakage current. In practice, this value translates into a reduction of the leakage current by 8–10% per degree centigrade in the temperature range from RT to $-20\,^{\circ}\text{C}$.

Leakage current: Annealing effects and parameterization

The annealing behaviour of the current related damage factor α after irradiation is displayed in Fig. 3 (right) for various annealing temperatures ranging from 21–106 °C [17]. The annealing temperature is the temperature at which the samples are stored or heated to accelerate the defect reactions in the silicon bulk. This temperature shall not be confused with the measurement temperature of the leakage current, which, in the given example, is 20 °C. The α value is continuously decreasing with increasing annealing time. In Refs. [16, 17] a parametrization of the data with an exponential and logarithmic term is proposed

$$\alpha = \alpha_1 \cdot \exp\left(-t/\tau_1\right) + \alpha_0 - \alpha_2 \cdot \ln\left(t/t_0\right) , \tag{11}$$

and has been used in the figure to fit the data (solid lines). The complete parameter set (α_0, α_1, α_2, τ_1, and t_0) and a discussion on the physical meaning of the parameters can be found in Refs. [16, 17].

2.1.3.2 Depletion voltage – space charge – effective doping concentration

The radiation induced defects lead to a change in the effective space charge N_{eff} that is reflected in a change of the depletion voltage V_{dep} of silicon detectors. The depletion voltage V_{dep} is given by

$$V_{\text{dep}} = \frac{q \cdot |N_{\text{eff}}| \cdot d^2}{2 \cdot \epsilon\epsilon_0} , \tag{12}$$

where d is the thickness of the device, q the elementary charge, ϵ the relative permittivity of silicon, and ϵ_0 the vacuum permittivity. It shall be noted that Eq. 12 assumes a constant space charge over the volume of the damaged detector, which is not always the case [21]. Furthermore, the depletion voltage is usually determined from capacitance vs. voltage (CV) measurements at ≈ 10 kHz and a temperature between $+20\,^{\circ}\text{C}$ and $-20\,^{\circ}\text{C}$ depending on measurement limits set by the high leakage currents, while a dependence of the depletion voltage on the measurement frequency and temperature has been reported for damaged detectors [22]. It is thus understood that the following parameterizations give precise values for the prediction of the depletion voltage (i.e., the kink in the CV measurement of a diode), while the translation into N_{eff} via Eq. 12 might be afflicted with systematic errors. It shall be mentioned that, in highly irradiated detectors, contrary to undamaged detectors, the space charge is no longer identical to the free carrier concentration in thermal equilibrium. Results of characterization methods determining the free carrier density or the low voltage resistivity are therefore not easily correlated with the space charge determined from full depletion voltage.

Depletion voltage: Fluence dependence

Figure 4 (left) shows an example of the evolution of the effective space charge (i.e., depletion voltage) for an n-type sensor with particle fluence [23]. Before irradiation the sensor was of high resistivity n-type (phosphorus doped) base material resulting in a positive space charge of some 10^{11} cm^{-3}. Irradiation of the sensor results in the formation of negative space charge, which compensates the initial positive

space charge. With increasing particle fluence, the net space charge decreases and reaches very low values corresponding to almost intrinsic silicon. This point is called *type inversion* or *space charge sign inversion (SCSI)*, as the space charge sign changes from positive to negative. Increasing the particle fluence beyond the SCSI point leads to more and more negative space charge values. The depletion voltage rises accordingly and eventually reaches values that cannot be applied to the detector any more without causing breakdown. The applied voltage will have to be kept below the depletion voltage and the detector is operated "underdepleted".
For high resistivity p-type sensors no "type inversion" is usually observed as the initial space charge is already negative before irradiation. It should, however, be mentioned that, after neutron and charged hadron irradiations, cases have been observed in non-standard silicon materials where type inversion occurs from negative to positive space charge [16] or the effective space charge remains positive in n-type sensors up to very high particle fluences [24, 25].

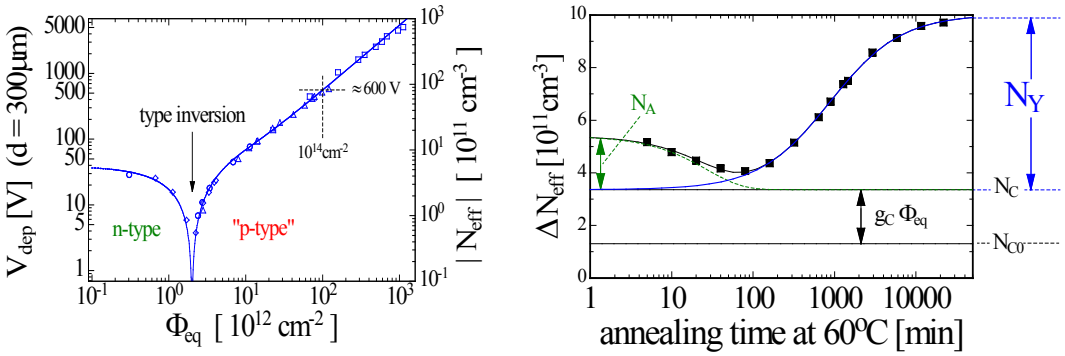

Fig. 4: Left: Effective doping concentration (depletion voltage) as a function of particle fluence for a standard float zone (FZ) n-type silicon detector. Data were measured directly after exposure and are taken from Ref. [23]. Right: Evolution of the effective doping concentration as function of annealing time. The data shown here were taken at room temperature while the annealing took place at 60 °C. Taken from Ref. [16].

Depletion voltage: Annealing and parameterization

The effective doping concentration after irradiation is changing with time. This so-called annealing can be accelerated at elevated temperatures and decelerated or frozen when going to lower temperatures. Figure 4 (right) gives an example for a typical annealing behaviour after high fluence irradiation. The change of the effective doping concentration with irradiation ΔN_{eff} is given by

$$\Delta N_{\text{eff}} = N_{\text{eff},0} - N_{\text{eff}}(t)\,, \tag{13}$$

where $N_{eff,0}$ is the value before irradiation and $N_{\text{eff}}(t)$ the value after irradiation. The fact that ΔN_{eff} is positive for the data shown in Fig. 4 (right) demonstrates that the radiation induced change of N_{eff} has a negative sign, i.e., the overall produced space charge due to radiation is a negative one, in accordance with the data shown in Fig. 4 (left). The time dependence of N_{eff} can be parameterized as

$$\Delta N_{\text{eff}}(t) = N_A(t) + N_C + N_Y(t)\,, \tag{14}$$

where N_C is the so-called *stable damage* component, which is not changing with time after irradiation, N_A is the *short term* or beneficial annealing component, and N_Y the *reverse annealing* component. They are parameterized as

$$N_A(t) \;=\; g_a \phi_{\text{eq}} \exp(-t/\tau_a) \tag{15}$$

$$N_C = N_{C,0}\,(1-\exp(-c\phi_{\rm eq})) + g_c\phi_{\rm eq} \quad (16)$$
$$N_Y(t) = g_y\phi_{\rm eq}(1-\exp(-t/\tau_y))\,. \quad (17)$$

Here, $N_{C,0}$ represents the fact that often an incomplete doping removal is observed (i.e., $N_{C,0}$ represents only a fraction of the initial doping concentration, see e.g., Ref. [26]), c is the removal coefficient, and g_a, g_c, and g_y are the introduction rates for the space charge defined as the beneficial annealing, the stable damage, and the reverse annealing above (e.g., $N_Y = g_y\phi_{\rm eq}$). The temperature dependence of the time constants for the beneficial (τ_a) and the reverse annealing (τ_y) has been found to follow an Arrhenius equation with activation energies of 1.09 eV and 1.33 eV, respectively [16]. Note as well that there are different parameterizations for the reverse annealing represented here by Eq. 17 (see e.g., Refs. [16, 24, 26]).

Depletion voltage: Material and particle dependence

Material and defect engineering techniques have been extensively studied by the RD48 [28] and RD50 [29] research collaborations in order to explore the potential for radiation hardening of silicon sensors. A wide range of sensors produced on different silicon base materials (e.g., different growth methods or different impurity content), exposed to different types of particles (e.g., electrons, pions, protons, and neutrons), and tested under various operational conditions (e.g., different temperatures and/or applied voltages during and after irradiation) have been studied. Particularly the enrichment of silicon with oxygen was studied in detail and found to be a key element for the radiation hardness of silicon sensors [27]. These studies demonstrated that the impurity content of the used silicon and the type of particle used for the irradiation experiment have a strong impact on the observed radiation damage and specifically on the space charge and the electric field distribution within the sensor. These findings demonstrate a weakness of the NIEL hypothesis, as the damage is no longer scaling for all silicon materials in the same way with the 1 MeV neutron equivalent fluence. An example is given in Fig. 5 (from Ref. [27]) showing data obtained on various n-type silicon detectors in a so-called *CERN scenario measurement* technique [30] where individual samples are successively exposed to radiation with annealing steps and measurements in between each irradiation step. The minimum in the curves for $|N_{\rm eff}|$ displays the fluence for which the material undergoes space charge sign inversion from positive to negative space charge from whereon the increase at higher fluence values is almost linear. The slope of this branch can be seen as a measure of the radiation hardness. Although oxygenated material does not exhibit any benefit for neutron irradiation (see Fig. 5 (left), it clearly leads to superior results with respect to standard FZ silicon in the case of proton or pion induced damage. Following the developments of the RD48 collaboration and the positive results on oxygen enriched silicon, the ATLAS and CMS pixel detectors at the LHC have been made from oxygen enriched silicon [31].

Depletion voltage: Donor removal

By the term donor removal we understand the transformation of electrically active shallow donors (usually phosphorus) into defect complexes that no longer have the properties of those shallow dopants. The positive space charge contributed by the shallow dopants is therefore lost and the overall space charge is altered. In the context of the depletion voltage, the donor removal is parameterized in the parameter N_C in Eq. 16), where an exponential function with a removal parameter c describes the fluence dependence. The removal of phosphorus and boron by irradiation with fast neutrons has been measured by Wunstorf *et al.* [32] using different high resistivity silicon wafers that were partly doped by the neutron transmutation doping (NTD) technique. From the measurement of the resistivity change as a function of the neutron fluence, removal coefficients were determined to be $c_D = 2.4 \times 10^{-13}$ cm^2 for phosphorus in very high resistivity n-type material (> 1 kΩcm). A systematic investigation of the dependence of the donor removal coefficient determined from space charge measurements on the phosphorus content (material resistivity) [26] revealed that the product of removal coefficient and phosphorus concentration

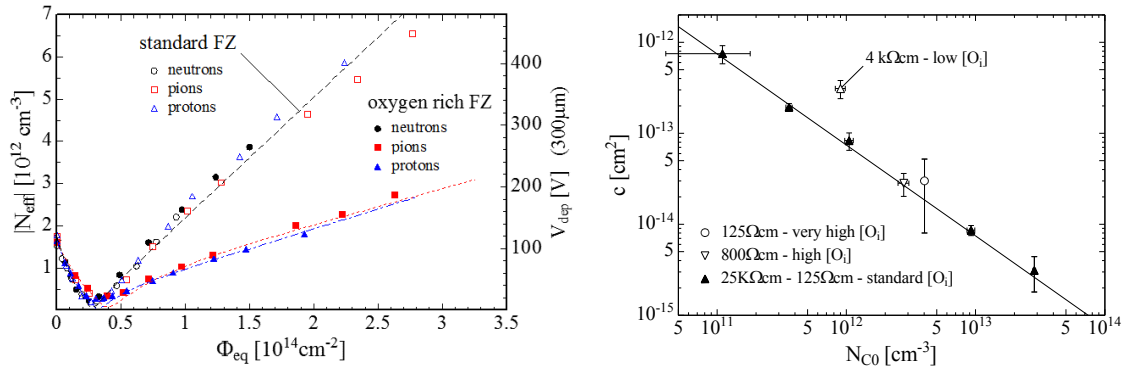

Fig. 5: Left: Dependence of N_{eff} on the accumulated 1 MeV neutron equivalent fluence for standard and oxygen enriched FZ silicon irradiated with reactor neutrons (Ljubljana), 24 GeV protons (CERN PS), and 192 MeV pions (PSI). Data of the RD48 collaboration taken from Ref. [27]. Right: Donor removal coefficient c plotted versus the donor concentration N_{c0} [26].

gives a constant value for materials varying over several orders of magnitude in resistivity. This is shown in Fig. 5 (right) and allows us to simulate this effect after neutron irradiations. For charged particle irradiations less data are available, but based on the nature of the removal mechanism and recent experiments on the acceptor removal in p-type silicon [33], a higher removal coefficient with respect to the one after neutron irradiation is expected.

2.1.3.3 Charge carrier trapping

The charge carriers generated by ionizing particles or photons in the depleted bulk of the silicon sensor travel towards the electrodes and constitute the sensor signal. If a charge carrier is trapped into a defect level and not released within the signal collection time of the sensor, the charge is lost and the corresponding sensor signal reduced.

Charge carrier trapping: Fluence dependence

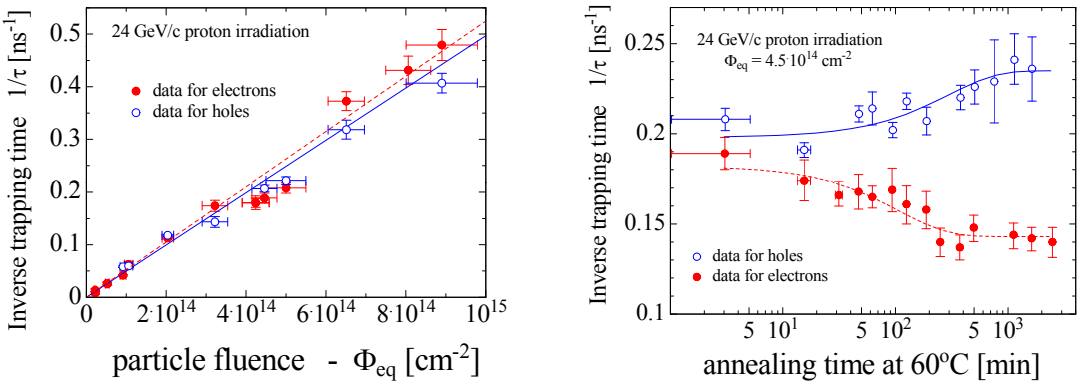

Fig. 6: Left: Inverse trapping time as a function of particle fluence as measured at 0 °C after an annealing of 30 to 60 min at 60 °C. Right: Evolution of the inverse trapping time as a function of annealing time at 60 °C. Data for both plots taken from Ref. [34] .

With increasing particle fluence (increasing number of trapping centres) more and more charge carriers get trapped during signal formation, leading to a decrease of the charge collection efficiency

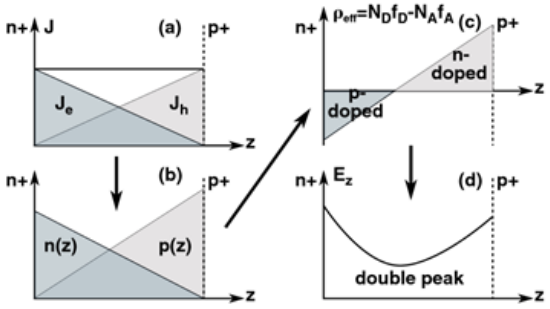

Fig. 7: The diagrams illustrate the polarization effect leading to a double peak electric field distribution in a sensor with a high defect concentration. (a) Current density distribution due to the generation of leakage current. (b) Carrier density distribution with higher hole concentration due to lower hole mobility. (c) Distribution of space charge due to predominant trapping of electrons close to the n^+ contact and holes close to the p^+ contact. (d) Distribution of electric field strength arising out of space charge distribution given in (c) (see Ref. [21] for more details).

(CCE) i.e., signal height of the sensor. The effective trapping time τ_{eff} can be used to describe this effect, assuming that the loss of charge depends uniquely on the transport time of the charge carriers inside the sensor: $Q(t) = Q_0 \exp(-t/\tau_{\text{eff}})$. The effective trapping time can be separately measured for electrons and holes [34, 35]. As shown in Fig. 6, a linear dependence of the inverse effective trapping time on the particle fluence is observed and can be described as

$$1/\tau_{\text{eff}} = 1/\tau_{(\text{eff},0)} + \beta\phi_{\text{eq}}\,, \tag{18}$$

where β is the proportionality factor (effective trapping damage constant) and $\tau_{\text{eff},0}$ the effective carrier lifetime before irradiation, which in standard silicon already after very moderate radiation levels can be neglected. Similar values for various silicon materials (float zone (FZ) [35], diffusion oxygenated FZ (DOFZ) [35], magnetic Czochralski (MCZ) [37], and epitaxial (EPI) [38]) and different heavy particle irradiations [35, 36] have been observed, resulting in β values of 4 to 6 $\times$ 10^{-16} cm^2/ns for electrons and 5 to 8 $\times$ 10^{-16} cm^2/ns for holes. In a more recent work focusing on high fluence irradiations, deviations from the linear behaviour shown in Fig. 6 (left) for particle fluences above about 3 $\times$ 10^{14} $\text{n}_{\text{eq}}\text{cm}^{-2}$ were reported [39]. The inverse trapping time (trapping rate) increased slower than expected from the linear extrapolation from low fluence data and gave e.g., a two to three times lower value at 3 $\times$ 10^{15} $\text{n}_{\text{eq}}\text{cm}^{-2}$.

Charge carrier trapping: Annealing

As for the leakage current and the depletion voltage (effective doping concentration), the effective trapping damage constant depends on the annealing status of the sensor after irradiation. This is depicted in Fig. 6 (right) for a proton irradiated sensor. While for electrons a reduction in β_e (decrease in $1/\tau_{\text{eff},e}$, less trapping) with annealing time is observed, for holes (damage parameter β_h) an increase of trapping with time has been measured. The trapping damage constant β has been parameterized for electrons and holes as

$$\beta(t) = \beta_0 \exp(-t/\tau_a) + \beta_\infty(1 - \exp(-t/\tau_a))\,, \tag{19}$$

where β_0 and β_∞ denote the trapping rates β at the beginning and end of the annealing process that is governed by the time constant τ_a [40].

2.1.4 The electric field and double junction effects

In the previous sections, and most importantly, in the transformation of the measured depletion voltage into effective space charge by Eq. 12, it is assumed that the space charge is homogeneously distributed

over the sensor bulk and constant. The electric field is thus assumed to be a linear function of the depth in the sensor. However, in reality this is often not the case and all results on the effective space charge as deduced from e.g., CV curves in form of depletion voltage characterization have to be treated with care. Only for non-irradiated sensors or low irradiation fluences can the space charge be assumed to be constant throughout the depleted sensor volume. For higher fluences, above about 10^{14} n_{eq}/cm^2, more complex field structures are observed. "Type inversion" or "space charge sign inversion (SCSI)" in an n-type sensor (see Section 2.1.3.2) was naively assumed to shift the space charge from positive to negative sign throughout the full sensor volume and consequently should lead to an electric field that starts to grow from the back electrode when rising the reverse bias over the sensor. While a strong electric field growing from the backside of the device is indeed observed, also a field growing from the front side is observed at the same time. The formation of such a double peak field structure can be explained by a polarization effect [21] and is illustrated in Fig. 7. The free carriers (electrons and holes) generated by radiation induced defects constitute the radiation induced leakage current. As electrons are drifting towards the n^+ electrode and holes towards the p^+ electrode, the electron density is highest at the n^+ contact while the hole density is highest at the p^+ contact (see Fig. 7b). The free carriers (electrons and holes) are partly trapped at radiation induced defect levels (acceptors and donors) and thus build up additional space charge. This space charge is predominantly negative at the n^+ contact and positive at the p^+ contact (see Fig. 7c). Finally, if the total effective space charge is negative at the n^+ contact and positive at the p^+ contact, a double peak electric field distribution is observed (see Fig. 7d).
The transient current technique (TCT) allows us to characterize and visualize the electric field distribution [41–43]. An example for a non-irradiated and highly irradiated sensor, as measured with edge TCT, is given in Fig. 8 [44]. The depth profiles of the sum of the drift velocities of electrons (ν_e) and holes (ν_h) as created in the indicated depth of the sensor is shown. This parameter relates to the electric field strength E via $\vec{\nu}_e + \vec{\nu}_h = \mu_e(E)\vec{E} + \mu_h(E)\vec{E}$ where $\mu_{e,h}$ are the carrier mobilities. In cases where the drift velocity has not saturated as a function of electric field strength, the sum of the drift velocities gives an image of the electric field strength within the sensor. It is clearly visible that the electric field in the non-irradiated sensor is growing from the front side while in the irradiated sensor fields are growing from both sides with rising reverse bias voltage. While many measurements on the electric field distribution

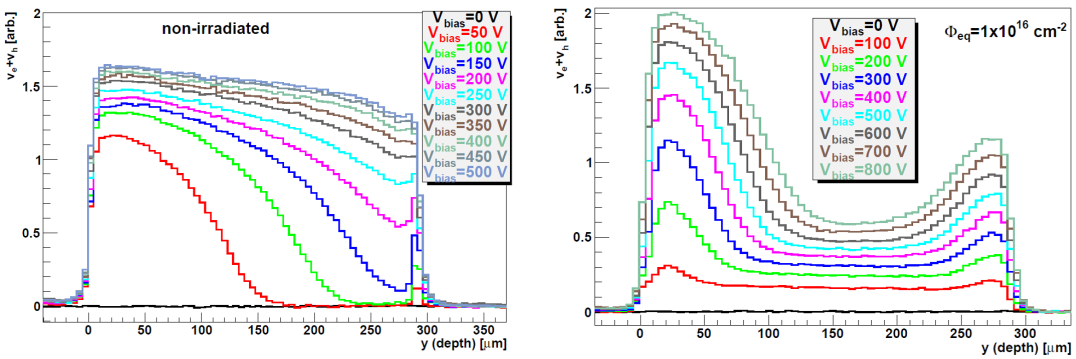

Fig. 8: Drift velocity profiles with varying bias voltages for a non-irradiated (left) and a neutron irradiated (10^{16} cm^{-2}) (right) p-type micro-strip detector made from float zone silicon (5 kΩcm, 300 μm, V_{dep}=180 V) . Figures taken from Ref. [44].

of irradiated sensors exist, a parameterization of the electric field distribution as a function of silicon material, particle fluence and type, sensor thickness, temperature, and annealing time does not exist to the same comprehensive level as e.g., for the effective space charge distribution presented in Section 2.1.3.2. A proposal on how to parameterize the electric field distribution has been made [44], but needs to be completed with a bigger set of measured data. Another approach to predict the electric field distribution as a function of the above mentioned parameters is to use TCAD simulations. Here, the defect levels

are parameterized and the electric field is calculated, offering the advantage that the parameterization becomes sensor geometry independent (see Chapter 7).

2.2 Electronics

It is of paramount importance to understand how radiation impacts the operation of microelectronic systems in the LHC experiment radiation environments so that electronics satisfying the reliability requirements can be designed, tested and qualified. Furthermore, the selection and qualification of commercial-off-the-shelf (COTS) electronics requires a good understanding of how they will perform in radiation environments for which they were not necessarily designed. The radiation quantities, listed below, are obtained from the Monte Carlo simulations described in Section 4. A difficulty arises, however, in that the radiation response of CMOS and bipolar electronics can depend strongly on the particle type and energy, dose rate, temperature, and bias. Reproducing all these conditions in test facilities is not feasible so the challenge is to relate the results to the real life application. The performance of microelectronic devices is impacted by radiation in several ways.

1. Total ionizing dose (TID) effects. This kind of damage accumulates over time causing device degradation and even failure. TID damage is associated with the build up of trapped charge states, either in an oxide layer or at the oxide–bulk (SiO_2-Si) interface, which leads to the modification of the electric fields in the device, thus impacting the electrical characteristics. In metal-oxide-semiconductor (MOS) transistors, the main parameters influenced by TID are the threshold voltage, charge mobility and leakage current. An example of a MOS transistor device structure is shown in Fig. 9. TID is measured in Grays (Gy) and values for the LHC experiments range from a few Gy up to several MGy. The discussion of TID effects in electronics at the LHC is continued below in Section 2.2.1.
2. Single event effects (SEE). When an ionizing particle deposits sufficient charge in a sensitive node, for example the drain in Fig. 9, then its normal function can be disrupted. A simple example is when a '1' is changed to a '0' (or vice versa) in a logic circuit or memory cell. Unlike TID and NIEL effects, SEEs are instantaneous and correlate strongly with the particle flux, itself proportional in LHC to the beam collision rate. The SEE sensitivity of a chip to radiation is defined by a cross-section, or the ratio between the events and the particle integrated flux triggering them, that is measured in an irradiation facility with the appropriate particle type and energy. At the LHC this cross-section is combined with the hadron fluence rate > 20 MeV to predict the rate of SEEs during operation [47]. The discussion of SEE effects in electronics at the LHC is continued below in Section 2.2.2
3. Non-ionizing energy loss effects, a cumulative degradation effect also known as displacement damage. Particles interacting in the semiconductor material cause atoms to be displaced, creating defects and clusters of defects in the crystal lattice and changes to the device electrical and optical properties. The accumulation of NIEL defects gives rise to effects such as increased leakage currents and changes in the effective doping concentrations. CMOS devices are typically less sensitive to NIEL effects compared with TID, mainly due to the high level of majority charge carrier doping. However, in some MOS devices with low doping features such as LDMOS (laterally diffused MOS), the impact of NIEL can play an important role. Bipolar electronics are typically more sensitive to bulk defects than CMOS. A full overview of displacement damage in silicon devices was given previously in Section 2.1.3.

2.2.1 TID effects

Electrons and holes are generated (in pairs) by ionizing radiation and normally transported in a device through the usual mechanisms of diffusion and drift. However, in the insulating oxide layers charges are

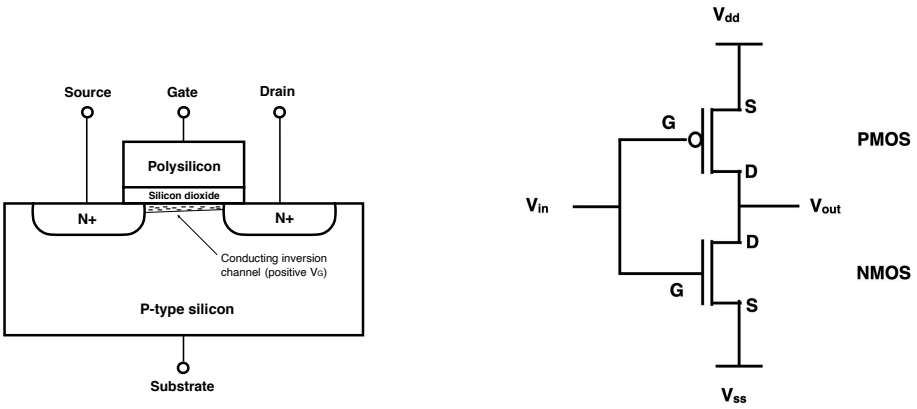

Fig. 9: Left: Schematic 2D representation of an NMOS transistor with N-type implants in a P-type body, creating two PN junctions. The SiO_2 is a thin insulating layer separating the P-type silicon bulk from the conductive polysilicon where the gate voltage is applied. A positive gate voltage induces the formation of a conduction n-channel at the SiO_2 interface where current can flow between source and drain in the presence of a horizontal electric field. The accumulation of radiation induced charged traps near the interface can significantly modify the conduction channel behaviour. Right: The combination of one NMOS and one PMOS transistor yields the simplest digital circuit: CMOS inverter. (G = gate; S = source; D = Drain.) When V_{in} is high, the NMOS transistor is switched on and current flows between the source and drain, and V_{out} takes the value of V_{ss}. When V_{in} is low, the NMOS transistor is off and V_{out} takes the value of V_{dd}. Both TID and SEE effects in either of the transistors can drastically impact circuit functionality.

less mobile than in the doped semiconductor regions. This is especially true for holes, which become trapped by defects in the oxide layer, resulting in an accumulation of positive charge during irradiation. The impact on CMOS and bipolar devices includes shifts in threshold voltages, opening of parasitic conductive paths (leakage currents) and decreased current gains. In CMOS structures (see Fig. 9) the migrating holes initiate a second class of defects close to the oxide–bulk interface which also leads to the degradation of the electrical performance. The physics behind oxide and interface charge trapping and annealing is complex, involving holes, protons (H+), and the breaking of Si–H bonds at the oxide–bulk interface [45]. The build up and annealing of these two kinds of effects is not the same and device performance is usually dose-rate and temperature dependent. An (infamous) example of the different kinetics of the two defects is the evolution of the leakage current during TID exposure. In many CMOS technologies the evolution of the leakage flowing between the drain and the source of the NMOS transistors has a non-monotonic behaviour, appearing as a 'bump' in a plot of leakage vs. TID (Fig. 10). After an initial increase, observed at low and moderate doses, the leakage current recovers when the TID is increased further. The height of the leakage current bump depends on the temperature and dose rate of the test, as well as the applied bias voltage. The peak of the bump is normally larger when the devices are kept cold. Because of this non-monotonic behaviour, it is strongly recommended to constantly monitor the evolution of the electrical characteristics of the circuits during radiation hardness assurance (RHA) irradiation tests, or at least to perform step-by-step irradiations. A case where this procedure was not followed is illustrated in Section 6.1.1, and as a consequence the increase of the system power consumption during data taking appeared as a surprise.

Ideally, when qualifying electronic components for TID in LHC radiation environments, whether ASIC or COTS, tests would be performed in similar radiation and environmental conditions. While this may be possible for temperature and biasing, irradiations have to be done on much shorter timescales than the lifetime of the detector systems, which means much higher dose rates. The consequence of

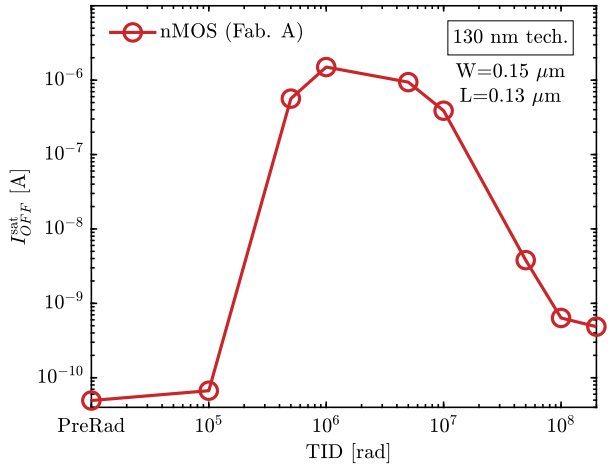

Fig. 10: Evolution of the source–drain leakage current in an NMOS transistor in 130 nm CMOS during a TID exposure. The position (in TID) and amplitude of the leakage depends on the temperature, bias, and dose rate.

using high dose rates on device performance is discussed below in Section 2.2.1.1. In addition to low dose-rate (LDR) effects, experiments also need to consider the sensitivity of TID response in different wafer production batches, which is discussed in Section 2.2.1.2. As a final comment on TID effects to electronics, we consider in Section 2.2.2.1 radiation effects on more recent technologies being used for the experiment upgrades.

2.2.1.1 LDR effects

The LDR effect refers to the fact that, for many components, the damage due to TID depends not only on the total dose, but also on the dose rate. The lifetime of a detector system may be up to ten years, which means TID testing at irradiation facilities has to be done with dose rates much higher than those found in the LHC radiation environments. In bipolar transistors, and in particular the older linear bipolar technologies, TID damage is typically larger for lower dose rates. This is a real LDR effect, named ELDRS (enhanced LDR sensitivity), that cannot be understood in terms of time evolution of defects and which makes it difficult to relate the laboratory results to the real life application. On the contrary, CMOS components were considered immune to real LDR effects, and by applying a post irradiation annealing procedure, known as a rebound test (168 h at 100 °C under bias), a reasonable prediction of the long term behaviour at lower dose rates could be established. An example of dose rate dependence in a CMOS device is illustrated in Fig. 11. Irradiating at high dose rates tends to lead to a negative shift in the threshold voltage because the build up of oxide-trap charge dominates. Irradiating at lower dose rates allows the oxide traps more time to anneal and at very low dose rates the impact of the interface-raps becomes dominant along with positive shifts in the threshold voltage.

Test methods have been developed for radiation hardness assurance (RHA) to take into account LDR effects [45]. Because of ELDRS, qualification of bipolar components is more challenging and the required test procedures more complex. In ATLAS, for example, testing on CMOS devices was derived from the MIL-STD 883-D Test Method 1019.4, a relatively straightforward method which includes the ‘rebound test’ (168 h at 100 °C with the device biased). The general idea of MIL-STD 883-D is to give a conservative upper bound to the effect of both oxide trapped charge and interface defects on the CMOS devices described above. Recommendations on test sample sizes are also given.

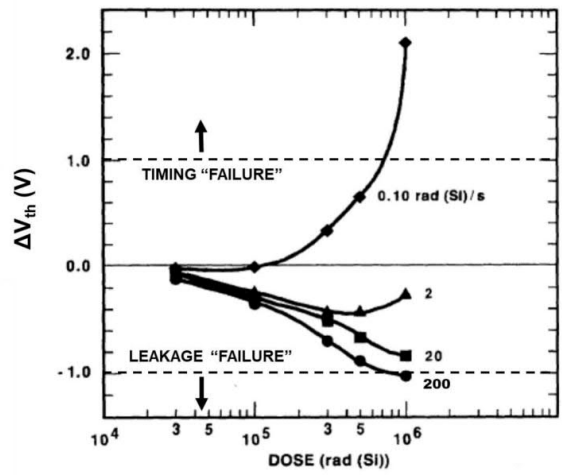

Fig. 11: Example of dose-rate dependence. Plot taken from Ref. [46].

2.2.1.2 Lot-to-lot effects

ASICs are designed in a specific technology process and can only be manufactured by a single company, although in several production plants (foundries). This decreases the possible variability in their radiation resistance, especially because it is typically possible to request fabrication at a specific plant. On the contrary, COTS components are most often purchased via a distributor and purchasing lots are constituted of samples of unknown origin. Unless specific agreements are concluded with the supplier to ensure a common and known origin of the components, a purchase lot has thus to be assumed inhomogeneous, i.e., components can come from different production lots. Measurements of samples coming from different manufacturing plants, or even from different lots produced at the same production site (Fab), have shown that relevant differences in the radiation damage might exist [49]. On top of the natural variability in their characteristics, normal even in very tightly controlled processes because of the incredible complexity of modern CMOS technologies, modifications to the processing sequence can be introduced by the manufacturer without warning. It is thus risky to assume comparable radiation response even for ASICs manufactured in the same Fab at different times. For COTS, of unknown origin, large variation can be found within the same purchase lot. It is therefore important to sample test for each batch or lot.

2.2.2 Single event effects

Single event effects (SEE) is the umbrella acronym covering a range of radiation effects on electronic circuits triggered by the transit of a single particle in the device [48]. These include single event upset (SEU), single event latch-up (SEL), single event gate rupture (SEGR), and single event burnout (SEB). For practical purposes we can also categorize the SEEs in terms of their impact on a system:

- soft SEEs (also called soft SEUs) are radiation induced bit flips that corrupt data or system configurations. They are not permanent effects as they can be dealt with by resetting the system or rewriting data in a memory. For example, a '1' can be changed into a '0' (or vice versa) in a combinatorial logic circuit, or in a register, or in a memory;
- hard SEEs (also called hard SEUs) are radiation induced bit flip that corrupts data or system configurations. They are permanent effects (they are not cancelled by resetting the system or rewriting data in a memory), such as a bit stuck to '1' in a memory cell;
- destructive SEEs (SELs, SEBs, SEGRs) lead to permanent damage. SELs are destructive SEEs, unless a robust architectural solution protects the circuit against thermal destruction resulting from latch-up. SEBs and SEGRs are always destructive SEEs typically affecting high-power and/or high-voltage circuits.

SEEs are caused by a single particle depositing a large amount of ionizing energy in a small sensitive region of the chip. For SEUs, the sensitive region is typically the drain of a transistor and the amount of charge required for the event is smaller than for the destructive SEEs. Since the sensitive region is very small, only particles with large linear energy transfer (LET) can trigger an event. In the CMOS generations used in LHC experiments, only nuclear fragments originating from hadronic collisions of the incoming particles (protons, neutrons, pions) with atoms composing the circuit can lead to a sufficient charge deposition. These fragments have a range of only a few micrometres in silicon, and they must hence be produced very close to the sensitive region.

With continuously decreasing feature size and lower operating voltages integrated circuits become sensitive to smaller amount of deposited charge. In terms of SEU rates, this, however, is compensated by the fact that the size of the sensitive region also decreases. Thus both the probability of a fragment traversing the sensitive region and its path length within this, decrease. As a net effect, the SEU cross-section per unit of digital value stored in the chip (for instance, per memory cell) has been observed to rather decrease with decreasing feature size. There is, however, another effect that should be considered: with a smaller charge needed to create the upset it is possible that fragments with lower energy or charge are sufficient to induce it. This might increase the SEU vulnerability of modern chips more sensitive to low-energy neutron interactions. Finally, even if the SEU cross-section per node decreases, the SEU cross-section per chip will increase drastically due to the increasing node density.

2.2.2.1 Evolution of electronics

Microelectronics has advanced enormously over the past 20 years, with feature sizes and oxide thicknesses having become much smaller. The original LHC ASICs that are now participating in the data taking were designed and manufactured mainly in a commercial-grade 250 nm process or in the dedicated radiation-tolerant DMILL technology. The LHC upgrades are now adopting more advanced commercial-grade CMOS technologies for the development of ASICs needing an order of magnitude more radiation tolerance, and a large effort in the characterization of the radiation effects in CMOS nodes ranging from 250 to 28 nm has been recently made. New effects have been reported, in particular (but not only) in 130 and 65 nm technologies exposed to ultra-high TID levels. Time-, bias-, and temperature-driven effects have been better understood, along with ELDR effects, and the systematic observation of effects in test structures manufactured in several production plants has provided essential data on the variability of the radiation effects. This new knowledge drives the need for modifying aspects of testing components at the LHC upgrades [49–51].

2.3 Optoelectronics

The effects of radiation on optoelectronics used at the LHC can be divided into radiation damage degrading the performance of optical links and single event effects (SEE).

2.3.1 Radiation damage and optoelectronics

The effects of radiation damage mechanisms in p-i-n diodes (p-type - insulator - n-type) are similar to those in semiconductor detectors (e.g., silicon microstrip sensors) as described in the subsections above). The creation of mid-band states in the depleted region of the p-i-n diode leads to an increase in leakage current. As the volume of the p-i-n diode is very much smaller than that of a silicon strip, this leakage current is not expected to create a significant problem for LHC optoelectronics. The radiation damage will create defects which can lead to charge trapping. As the thickness of the depletion layer in the p-i-n diode is much less than that of typical silicon detectors this effect is also not expected to lead to significant signal loss for LHC applications. Finally the radiation damage will create defects in the active region of the p-i-n diode which will lead to the creation of acceptor states and therefore change the effective charge

carrier density which will cause the full depletion voltage to increase. However, if the bias voltage can be maintained at a value greater than the full depletion voltage this effect will not cause any signal loss.

The radiation damage in a Vertical Cavity Surface Emitting Laser (VCSEL) arises from bulk damage leading to defects which act as non-radiative recombination centres [52]. These decrease the minority carrier lifetime and hence the fraction of radiative transitions. This is a small effect for VCSELs operated above laser threshold as in this region they are dominated by stimulated emission with a correspondingly short lifetime. However, this is a significant effect below laser threshold because of the much longer lifetimes for spontaneous emission. This therefore can result in a significant increase in laser threshold. Complex annealing processes occur in the VCSELs and this can be accelerated by the electron-hole currents [52]. This injection annealing can lead to a very large fraction of the initial radiation damage being removed. Very significant radiation damage effects have been observed in VCSELs and Edge Emitting Lasers (EEL) from test beam studies.

2.3.2 Single event effects

As already discussed in Section 2.2.2, an SEE occurs when a high energy particle deposits a sufficiently large amount of energy in a small volume of electronics. In principle the effect can lead to a catastrophic failure but more commonly it can cause a bit to flip in a Single Event Upset (SEU). SEUs have been observed in LHC operation. The most vulnerable component to SEU in optical links is the p-i-n photodiode as a small amount of energy deposited in the active region of this type of device is indistinguishable from the signal from the infra-red photons in the optical link.

In a typical application the energy deposited by a minimum ionizing particle (MIP) passing through a p-i-n photodiode will be below threshold for causing an SEU. The main origin of SEUs at the LHC is high energy hadrons making nuclear interactions upstream close to the p-i-n photodiode and the combination of the energy deposition from the secondary particles is sufficient to cause an SEU. This requires very detailed simulations to make predictions for SEU rates at LHC, see for example Ref. [5]. Note that this is very different to space applications in which SEUs arise mainly from slow moving heavy ions which can have large enough LET to create SEUs. SEUs in optical links can therefore be studied either with beams of high energy protons or pions or with heavy ion beams. Estimates of the SEU rates in LHC operation have been made and compared to extrapolations from test beam data. This report also discusses some simple mitigation strategies that have been used to minimize the loss of data from SEUs and gives estimates for the fraction of data lost due to SEUs. More sophisticated mitigation strategies are planned for the HL-LHC detector upgrades.

References

[1] A. Vasilescu and G. Lindström, Displacement damage in silicon, last accessed July 15 2020.

[2] P.J. Griffin *et al.*, SNL RML recommended dosimetry cross section compendium, SAND92-0094 (Sandia Natl. Lab., Albuquerque, NM, 1993), doi:10.2172/10115441.

[3] G.P. Summers *IEEE Trans. Nucl. Sci.* **40** (1993) 1372, doi:10.1109/23.273529.

[4] A.Yu. Konobeyev *et al.*, *J. Nucl. Mater.* **186** (1992) 117, doi:10.1016/0022-3115(92)90328-I.

[5] M. Huhtinen and P.A. Aarnio, *Nucl. Instrum. Meth.* **A335** (1993) 580, doi:10.1016/0168-9002(93)91246-J.

[6] M. Huhtinen, *Nucl. Instrum. Meth.* **A491** (2002) 194, doi:10.1016/S0168-9002(02)01227-5.

[7] C. Inguimbert *et al.*, *IEEE Trans. Nucl. Sci.* **57** (2010) 1915, doi:10.1109/TNS.2010.2049581.

[8] C. Inguimbert and S.R. Messenger, *IEEE Trans. Nucl. Sci.* **59** 3117, doi:10.1109/TNS.2012.2221477.

[9] S.R. Messenger *et al.*, *Prog. Photovolt. Res. Appl.* **9** (2001) 103, doi:10.1002/pip.357.

[10] S.R. Messenger *et al.*, *IEEE Trans. Nucl. Sci.* **58** (2011) 3118, doi:10.1109/TNS.2011.2172957.

[11] R. Radu *et al.*, *Appl. Phys.* **117** (2015) 164503, doi:10.1063/1.4918924.

[12] S.M. Sze, *Semiconductor Devices: Physics and Technology*, 3rd ed. (Wiley, New York, NY, 2012), see chapter 3 for a brief summary of the Shockley-Read-Hall theory.

[13] M. Moll, *IEEE Trans. Nucl. Sci.* **65** (2018) 1561, doi:10.1109/TNS.2018.2819506.

[14] M. Moll *et al.*, *Nucl. Instrum. Meth.* **A426** (1999) 87, doi:10.1016/S0168-9002(98)01475-2.

[15] J.R. Srour and J.W. Palko, *IEEE Trans. Nucl. Sci.* **60** (2013) 1740, doi:10.1109/TNS.2013.2261316.

[16] M. Moll, Radiation damage in silicon particle detectors: Microscopic defects and macroscopic properties, PhD thesis: Hamburg University, 1999.

[17] M. Moll *et al.*, *Nucl. Instrum. Meth.* **B186** (2002) 100, doi:10.1016/S0168-583X(01)00866-7.

[18] I. Pintilie *et al.*, *Nucl. Instrum. Meth.* **A514** (2003) 18, doi:10.1016/j.nima.2003.08.079, DESY-02-199D.

[19] I. Pintilie *et al.*, *Nucl. Instrum. Meth.* **A611** (2009) 52, doi:10.1016/j.nima.2009.09.065, arXiv:0907.3050 [physics.ins-det].

[20] A. Chilingarov, *JINST* **8** (2013) P10003, doi:10.1088/1748-0221/8/10/P10003.

[21] V. Eremin *et al.*, *Nucl. Instrum. Meth.* **A476** (2002) 556, doi:10.1016/S0168-9002(01)01642-4.

[22] D. Campbell *et al.*, *Nucl. Instrum. Meth.* **A492** (2002) 402, doi:10.1016/S0168-9002(02)01353-0.

[23] R. Wunstorf, Systematische Untersuchung zur Strahlenresistenz von Silizium-Detektoren für die Verwendung in Hochenergiephysik-Experimenten, PhD thesis, Hamburg University, 1992.

[24] G. Lindström *et al.*, *Nucl. Instrum. Meth.* **A556** (2006) 451, doi:10.1016/j.nima.2005.10.103.

[25] N. Pacifico *et al.*, *Nucl. Instrum. Meth.* **A658** (2011) 55, doi:10.1016/j.nima.2011.03.026.

[26] M. Moll *et al.*, *Nucl. Instrum. Meth.* **A439** (2000) 282, doi:10.1016/S0168-9002(99)00842-6.

[27] G. Lindström *et al.*, *Nucl. Instrum. Meth.* **A466** (2001) 308, doi:10.1016/S0168-9002(01)00560-5.

[28] The ROSE Collaboration: CERN RD48, last accessed July 15 2020; F. Lemeilleur; Proposal for further work on radiation hardening of silicon detectors, CERN-LHCC-96-023, LHCC-P-62 (CERN, Geneva, 1996).

[29] D. Mauro De Palma *et al.* [RD50 Collaboration], Radiation hard semiconductor devices for very high luminosity colliders, CERN-LHCC-2002-003, LHCC-P-6 (CERN, Geneva, 2002).

[30] A. Ruzin [RD48 Collaboration], *Nucl. Instrum. Meth.* **A447** (2000) 116, doi:10.1016/S0168-9002(00)00179-0.

[31] F. Hartmann, *Evolution of Silicon Sensor Technology in Particle Physics*, 2nd ed. (Springer, Berlin, 2017), doi:10.1007/978-3-319-64436-3.

[32] R. Wunstorf *et. al.*, *Nucl. Instrum. Meth.* **A377** (1996) 228, doi:10.1016/0168-9002(96)00217-3.

[33] M. Moll, *PoS* **Vertex2019** (2020) 027, doi:10.22323/1.373.0027.

[34] O. Krasel *et al.*, *IEEE Trans. Nucl. Sci.* **51** (2004) 3055, doi:10.1109/TNS.2004.839096.

[35] G. Kramberger, *Nucl. Instrum. Meth.* **A481** (2002) 297, doi:10.1016/S0168-9002(01)01263-3.

[36] G. Kramberger, Solid state detectors for high radiation environments, in *Detectors for Particles and Radiation. Part 2: Systems and Applications, Landolt-Börnstein - Group I: Elementary Particles, Nuclei and Atoms, vol. 21B2*, Eds. C.W. Fabjan and H. Schopper (Springer, Berlin, 2011), chap. 7.2, doi:10.1007/978-3-642-14142-3_7.

[37] A.G. Bates and M. Moll, *Nucl. Instrum. Meth.* **A555** (2005) 113, doi:10.1016/j.nima.2005.09.020.

[38] J. Lange *et al.*, *Nucl. Instrum. Meth.* **A624** (2010) 405, doi:10.1016/j.nima.2009.11.082.

[39] W. Adam *et al.* [CMS Tracker Group], *JINST* **11** (2016) P04023, doi:10.1088/1748-0221/11/04/P04023.

[40] G. Kramberger, Signal development in irradiated silicon detectors, Ph.D. thesis, University of Ljubljana, 1998.

[41] V. Eremin *et al.*, *Nucl. Instrum. Meth.* **A372** (1996) 388, doi:10.1016/0168-9002(95)01295-8.
[42] G. Kramberger *et al.*, *IEEE Trans. Nucl. Sci.* **57** (2010) 2294, doi:10.1109/TNS.2010.2051957.
[43] M. Fernández García *et al.*, *JINST* **12** (2017) C01038, doi:10.1088/1748-0221/12/01/C01038.
[44] G. Kramberger *et al.*, *JINST* **9** (2014) P10016, doi:10.1088/1748-0221/9/10/P10016.
[45] J.R. Schwank *et al.*, *IEEE Trans. Nucl. Sci.* **55** (2008) 1833, doi:10.1109/TNS.2008.2001040.
[46] D.M. Fleetwood and H.A. Eisen, *IEEE Trans. Nucl. Sci.* **50** (2003) 552, doi:10.1109/TNS.2003.813130.
[47] M. Huhtinen and F. Faccio, *Nucl. Instrum. Meth.* **A450** (2000) 155, doi:10.1016/S0168-9002(00)00155-8.
[48] Edward Petersen, Single event effects in aerospace, Wiley-IEEE Press, 2011.
[49] F. Faccio et al, *IEEE Trans. Nucl. Sci.* **62** (2015) 2933 doi:10.1109/TNS.2015.2492778.
[50] F. Faccio et al, *IEEE Trans. Nucl. Sci.* **65** (2018) 164 doi:10.1109/TNS.2017.2760629.
[51] G. Borghello et al. *IEEE Trans. Nucl. Sci.* **65** (2018) 1482 doi:10.1109/TNS.2018.2828142.
[52] Teng, P. K. *et al.*, *Nucl. Instrum. Meth.* **A497** (2003) 294, doi:10.1016/S0168-9002(02)01922-8.